Chem. Chem. Technol., 2017,
Vol. 11, No. 1, pp. 25–34

Chemistry

STRUCTURAL, MORPHOLOGICAL AND OPTICAL PROPERTIES OF NANOPRODUCTS OF ZIRCONIUM TARGET LASER ABLATION IN WATER AND AQUEOUS SDS SOLUTIONS

Vyacheslav Karpukhin[1, *], Michael Malikov[1], Tatyana Borodina[1], George Valyano[1], Olesya Gololobova[1], Dmitry Strikanov[1]

DOI: dx.doi.org/10.23939/chcht11.01.025

Abstract. Structural, morphological and optical properties of nanoproducts of laser ablation of zirconium target in water and aqueous SDS solutions were investigated. Depending on experiment conditions the indicated products can appear as different crystalline phases of zirconia and organic-inorganic composites, which include SDS alkyl chains intercalated between layers of zirconium oxides or hydroxides. The formation of zirconium dioxide-based hollow nano and microstructures is demonstrated. It is suggested that ablation formed gas-vapor bubbles can serve as templets for generation of hollow structures.

Keywords: laser ablation, metal nanocompositions, ZrO_2, RAMAN spectra.

1. Introduction

Numerous publications devoted to both synthesis and investigation of properties of nano dispersed zirconia have appeared by now [1-8]. Such interest is determined by unique mechanical, chemical, optical, and other properties that open way to a broad practical application of the material in science and technology [9-13]. Synthesis of oxides and other metal nanocompositions by laser ablation in a liquid environment is one of promising methods [14-16]. However, the data on zirconia generation by the mentioned way is far not sufficient [17-21]. The experiments were carried out mainly at low laser pulses repetition rate (~ 10 Hz), that limits the chances of establishing productive technologies, potential investigations of a number of physical and chemical processes accompanying the synthesis and affecting properties of the final product.

Thus, the given work is devoted to the attempt of generating nanocrystalline zirconia by laser ablation of zirconium target in aqueous solutions of a surfactant. A copper vapor laser (CVL) with the power output of 10–15 W, radiation pulse duration of 20 ns, and pulse repetition rate of 10 kHz was used as radiation source.

2. Experimental

Physical and technical descriptions of laser ablation in liquid are given in detail in numerous original articles and reviews [22-26]. CVL generation was performed at two wave lengths: 510.6 and 578.2 nm; line power ratio was 2:1, respectively. UV light (255, 271 and 289 nm) was obtained by nonlinear conversion of the Cu laser radiation (510.6 and 578.2 nm) in a BBO crystal [27]. The laser beam was focused onto the target surface by an achromatic lens with focal distance of $f = 280$ mm, that provided the spot diameter of less than 100 μm. The target was placed into a glass cell with deionized water or aqueous solutions of a surfactant. The volume of the liquid in the cell was ~ 10 cm^3. The cell was placed in a vessel with cooling water and its temperature was kept at ~ 300 K. The vessel was installed on a movable table that permitted to constantly move the focal spot over the target surface. The surfactant SDS ($C_{12}H_{25}SO_4Na$) of anionic group was used for the experiment.

The optical characteristics of colloidal solutions with nanostructures of zirconia were analyzed by the absorption spectral method in the range of 200–700 nm by SF-46 spectrophotometer with automatic data processing. RAMAN Spectra were recorded by double monochromator KSVU-23. The structure and composition of the solid phase extracted from the colloid solution after centrifugation at 15000 rpm and evaporation at

[1] Joint Institute of High Temperatures, Russian Academy of Science13(2), Izhorskaya St., 125412 Moscow, Russian Federation
[*] *vtkarp@gmail.com*

320–330 K were analyzed at X-ray diffractometer DRON-2 (K_α copper line). Shapes and sizes of nanostructures were determined by Hitachi S405A scanning electron microscope at accelerating voltage of 15 kV, according to the standard technique.

3. Results and Discussion

3.1. XRD Data

The experiments were performed both in deionized water (SDS solution molarity M = 0) and at M = 0.0001, 0.01, 0.05 and 0.1. Exposition times of radiation onto the target τ_{exp} were varied within the intervals from 5 to 180 min. In a number of cases properties of colloid and its solid phase were analyzed tens hours later (the aging time). Fig. 1 demonstrated typical XRD patterns of solid phase of colloids at (M) SDS = 0 and 0.1. After ablation of zirconium in deionized water the synthesized zirconia was mainly in X-ray amorphous state, *i.e.* the size of the crystallites did not exceed 1–2 nm (*curve* 2). The crystalline part of the solid contains 5–9 vol % of monoclinic phase, 4 vol % of tetragonal phase and about 3 vol % of metal zirconium. Sizes of metal zirconium crystallites make not less than 100 nm, of monoclinic phase ~ 40–75 nm and of tetragonal phase ~ 60–100 nm. Sizes of nanoparticles become less with the increase of exposition time. Crystalline lattice parameters of dioxide tetragonal modification stay within the limits of a = 0.05083–0.5093 nm, c = 0.5127–0.5185 nm, with ratio c/a varying from 1.007 (close to cubic structure) to 1.019. It is supposed that ions of OH^- appearing in the process of ablation can serve as a stabilization factor for tetragonal phase at M = 0. It is supported in other similar experiments [28]. We can observe a tendency of extending monoclinic phase along with exposition time growth and reduction of metal zirconium amount.

At M = 0.01 a greater part of colloid solids is in the amorphous state as well. The crystalline part consists of SDS, monoclinic, tetragonal phases and a small part of metal zirconium. The ratio of monoclinic and tetragonal phases makes ~ 1.6:1. Lattice parameters of tetragonal phase are: a = 0.5115 nm, c = 0.5133 nm, *i.e*. the lattice is close to cubic. Sizes of monoclinic phase particles are 60–100 nm and 45–100 nm for tetragonal ones. The increase of ablation time up to 180 min enhances the crystalline part. The monoclinic phase makes about 8 vol %, the tetragonal phase is about 7 vol %. Tetragonal phase average size equals to about 60 nm, while that of monoclinic phase is about 80 nm. The increase of SDS concentration to M = 0.05 does not practically change XRD patterns structure. Similar to M = 0.01, about 2.5 vol % of zirconium is presented. Average size of particles for both parts of dioxide and metal zirconium reduces to 40–45 nm. The reduction of crystallite average sizes at M = 0.01 and 0.05 with regards to crystallite sizes at M = 0 is caused by the influence of surfactant - SDS, which restricts nanoparticles growth [29, 30]. The presence of SDS in the initial solution creates prerequisites for the appearance of the third high temperature phase of zirconia, *i.e.* a cubic phase. Thus, in experiments at M = 0.01, 0.05, 0.1 phases with lattice spacing of a = 0.5127 nm, 0.5115 nm and of c = 0.513 nm were presented, *i.e*. phases close to cubic ones. Tetragonal and cubic phases can be stabilized by anions OH^-, anions SO^-_2, SO^-_3, SO^-_4 of SDS which appear during ablation time, interact with crystalline surface and prevent oxygen penetration, as well as cations Na^+ [28]. At the concentration of SDS in solution up to M = 0.1 XRD patterns is observed as a spectrum of well crystallized SDS, a considerable part of which is oriented along the surface of glass plate (plane 00L), a smaller part is distributed chaotically (Fig. 1, *curve* 1). Along with lines belonging to SDS and ZrO_2 the XRD spectrum has a number of other maxima whose intensity considerably surpasses intensity of zirconia lines, though it is weaker than SDS maxima. Some of those lines can be attributed to hydrate $SDS{\cdot}H_2O$ and $Na_2S_2O_3{\cdot}H_2O$. The spectrum also clearly demonstrated the phase with interlayer distance d = 5.165 nm. Distances close to the indicated ones are typical of organic-inorganic composites with alkyl chains intercalated between oxide or hydroxide layers of transition metal Zn, Co, Fe, Cu, *etc*. [31]. The chains may be placed perpendicular to oxide or hydroxide layers and tilting, as well, besides, the chains are connected between themselves by hydrocarbon "tails". They may be partially interdigitated. Thus, formation of one-layer and two-layer structures with broad variation of parameter d ~ 0.25–6 nm is possible. The formulas of such compositions are as follows: $(M)_2(OH)_3X{\cdot}z{\cdot}H_2O$ and $(M)(OH)_2X{\cdot}z{\cdot}(H_2O)$ for hydroxides and $X{\cdot}M^{2+}{\cdot}z{\cdot}(H_2O)$; $X{\cdot}M_2\ O^{2+}{\cdot}z{\cdot}(H_2O)$ for oxides, where M is divalent metals (Zn, Cu, Zr), X is intercalated anion alkyl sulfate($C_nH_{2n+1}\ SO_4$, where n = 12), z is molecules number of H_2O [31, 32]. The authors have already obtained similar Zn and Cu composites during ablation of the indicated metal targets in aqueous SDS solutions [33].

Long exposition of radiation in colloid may cause breaking of SDS molecules, that formed new phases – b-$Zr(SO_4)_2$ and b-$Zr(SO_4)_2{\cdot}H_2O$ in the spectrum [34]. It should be emphasized that a specific feature of the experiment is predominance of synthesized zirconia in amorphous state mainly.

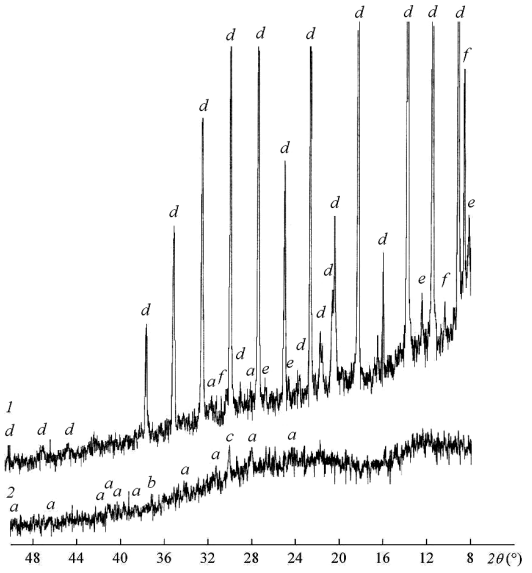

Fig. 1. X-ray diffraction patterns of precipitates extracted from the colloidal solution, depending on the (M) SDS concentration: 0 (2) and 0.1 (1). Phases: monoclinic zirconia (a); Zr (b); tetragonal zirconia (c); SDS (d); SDS·H_2O (e), system based on Zr and SDS (Zr-SDS nanocomposite) (f)

3.2. RAMAN Spectra

The spectrum obtained at M = 0 shows the presence of monoclinic, tetragonal and cubic phases of ZrO_2 in solid part of colloid (Fig. 2). While comparing the spectra taken at M = 0.1 and deionized water (Fig. 3), at M = 0.1 we see peaks in the region of 2000–2400 cm^{-1} and 2800–3000 cm^{-1}, that can be attributed to a vibrational structure of $Zr(OH)_4$ molecule. Fixation of zirconium oxide and hydroxide in RAMAN spectra at M ≥ 0.01 together with XRD data most obviously speaks in favor of synthesis of organic-inorganic composite Zr – SDS, consisting of zirconium oxide or hydroxide layers with intercalated SDS alkyl chains.

3.3. Morphology of Synthesized Products

Figs. 4 and 5 present images of solid phase structures of colloid at different t_{exp} and SDS solution molarity M. The treatment of samples synthesized in deionized water (M = 0) at t_{exp} = 5, 20, 180 min showed that they consist of separate large particles (up to 10 μm), aggregates of rounded particles (~ 100–500 nm) and dense mixture of grains with poorly defined boundaries (Fig. 4a). The latter ingredient of the microstructure is more typical for t_{exp} = = 180 min, where it is main, X-ray amorphous component. At t_{exp} = 5 and 20 min it can be observed in the structure among large and small particles spherical hollow units with sizes from tens nm to several μm, some of them concave and partially broken (Figs. 4b and 4c). The cover of large hollow particles consist of separate layers, the thickness of the cover can be within 50–200 nm and more (Figs. 4a and 4d). That correlates with the XRD data for an average size of nanoparticles (~40–100 nm) that build up microstructures.

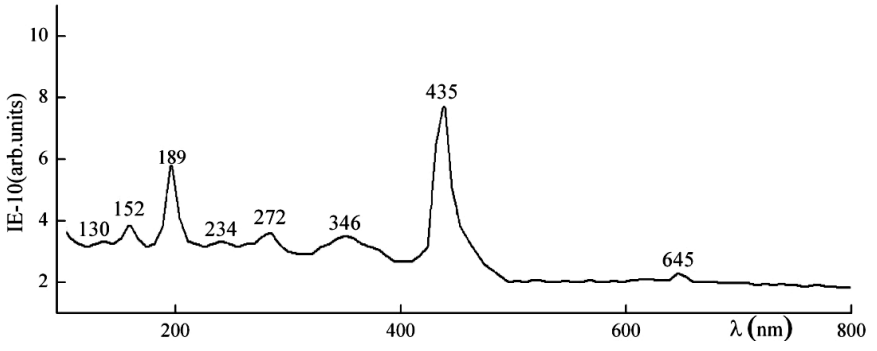

Fig. 2. Raman spectra of the precipitate colloid λ_{exc} = 510 nm. Phase ZrO_2: 130, 189, 346 – monoclinic; 152, 234, 272, 435 – tetragonal; 520 – 670 cubic

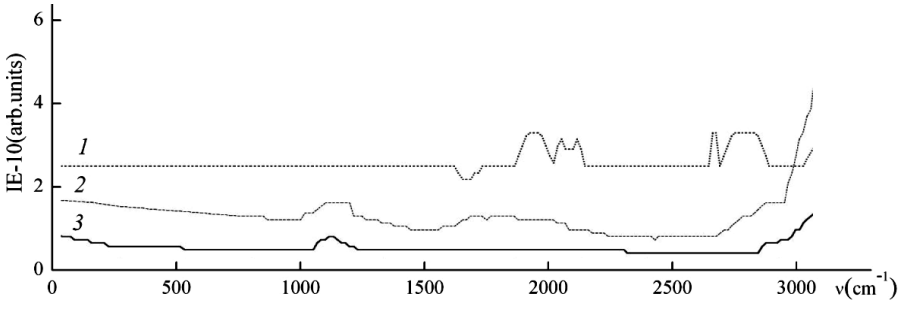

Fig. 3. Raman spectra of the precipitate colloid λ_{exc} = 271 nm, depending on the (M) SDS concentration: 0.1 (1); 0 (2) and H_2O (3). Range of 2000–2400 cm^{-1} – $Zr(OH)_4$; 2780–3000 cm^{-1} – $Zr(OH)_4$ and SDS

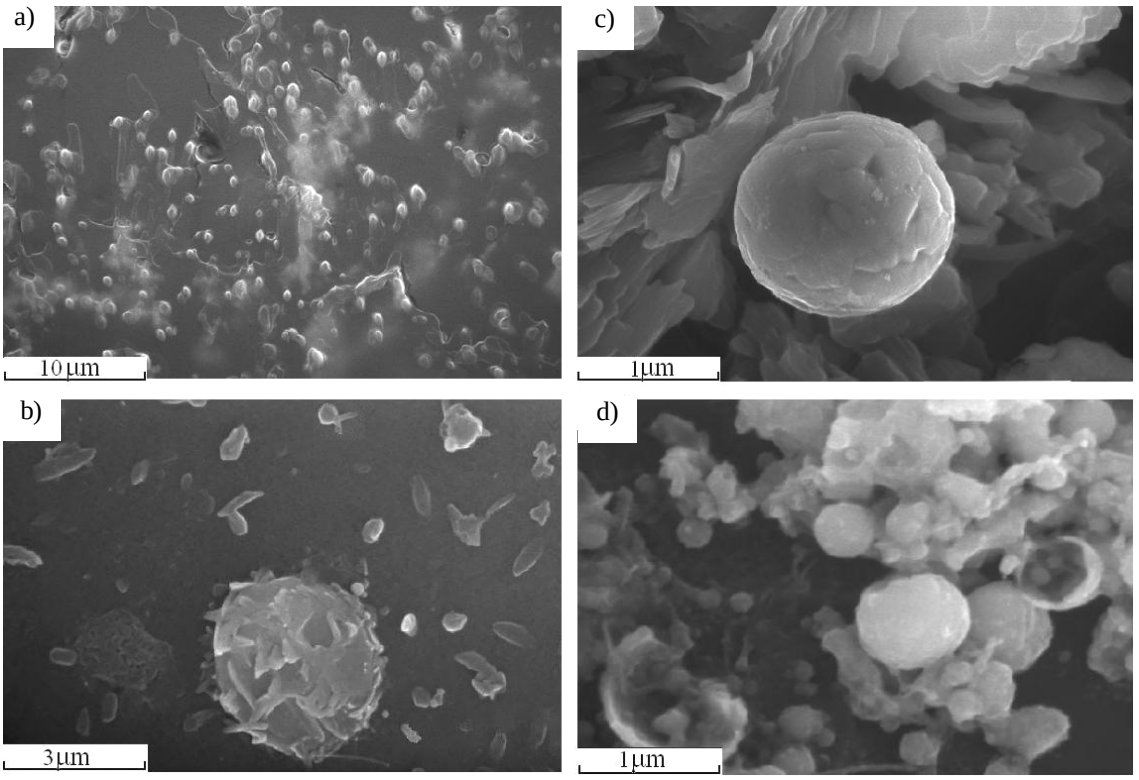

Fig. 4. Microstructure of the surface phase of the colloid obtained in the concentration (M) SDS = 0 M: t_{exp} = 180 min (a) and t_{exp} = 20 min (b-d)

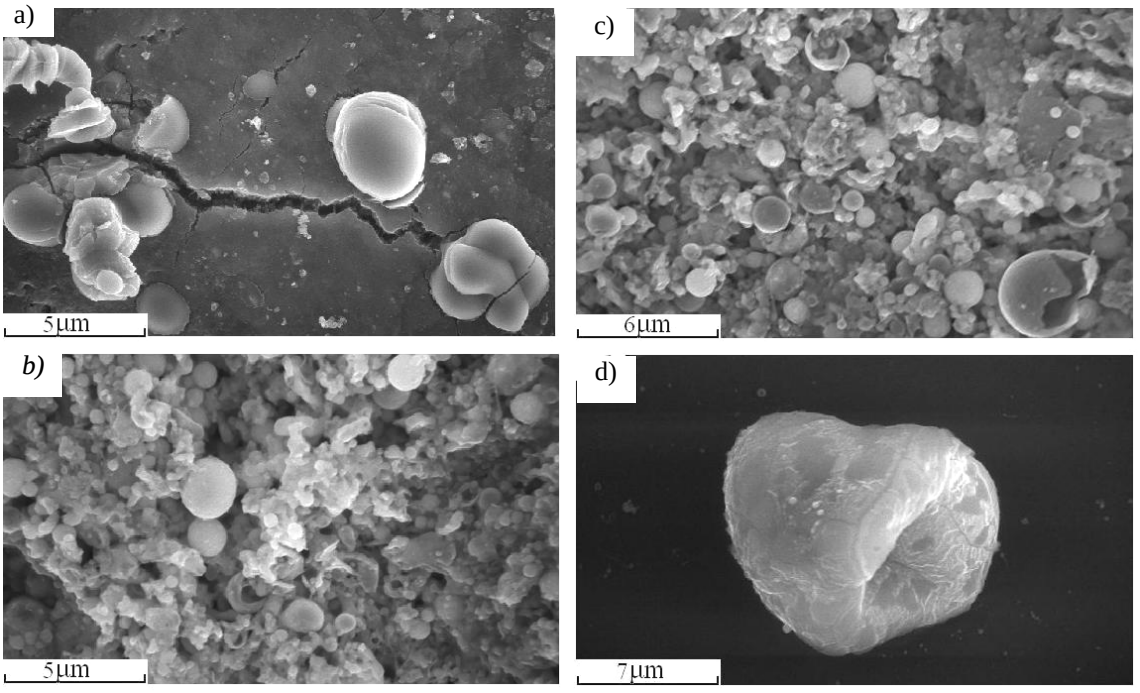

Fig. 5. The microstructure of the surface phase of the colloid obtained in the concentration M > 0: units of ZrO_2 (a); forming a shell of crystallites SDS (b); melted shell (c) and the structure of the "rattle" (d)

The crystalline part of the solid phase extracted from colloid is significantly changed when SDS is added to the initial solution. It is known that micellae (Hartley type) start to appear in the solution if SDS concentration exceeds the critical level (M ~ 0.008 mol/l). With the increase of M crystals begin to grow. In accordance with Wolf principle chain-like structure of SDS molecule predetermines that crystals are formed either as thin elongated plates for SDS anhydrite or monohydrite, or as octahedral-like plates for $C_{12}H_{25}OSO_3Na \cdot 1/8H_2O$ [35]. After aging of colloid for dozens hours the images show crystals in the shape of long sticks (Fig. 5b). The above-mentioned plate units may serve as templets to form laminar structures of organic-inorganic composites based on zirconium oxides or hydroxides. When exposition exceeds 5 min pictures show zones of crystallized SDS structures, areas of amorphous SDS and zirconia and droplets of aggregates or separate large solid and hollow zirconia nanoparticles.

Hollow nano and microspheres are observed at all regimes of zirconium target ablation both in deionized water and in SDS solution (Fig. 4c and 5d). However, at M = 0 average sizes of hollow particles are noticeably larger than at M ≥ 0.01. Some publications consider adsorption of nanoparticles on the surface of vapor-gas bubbles to be a basic mechanism for formation of hollow structures, *i.e.* the gas bubble serves as a "soft" templet [36-39]. There might be several reasons for bubble formation. There are certain zones in the focal spot on the target surface due to space and time power distribution over beam area: ablation ($\geq 10^8$ W/cm^2), melting ($< 10^8$ W/cm^2), surface heating above liquid boiling point [40]. The ablation produces a plasma-vapor-gas bubble; its collapse may create secondary gas (H_2, O_2) and vapor bubbles [40-44]. The process generates both heated solid particles and metal droplets with a vapor cloud around them [45]. Besides, in passing through the laser beam particles may get heated up to temperatures above the melting point, break to small fragments, which is accompanied by vapor bubbles formation [46]. The main reason for appearance of a solid shell on gas bubble surface is the adsorption of solid particles on the gas–liquid boundary (capillary effect). It leads to decrease of the surface energy of the bubble-particle system:

$$\Delta E = -pR^2 g\,(1-\cos q)^2$$

where R is a particle radius, γ is surface energy of a gas bubble (water–gas boundary), θ is a contact angle of the particle with the bubble surface.

Angle θ is < 90, as particles of metal oxides are hydrophilic. Calculation shows that for $R = 2$ nm, $\gamma \approx 74 \cdot 10^{-3}$ N/m and $\theta \approx 40^\circ$, $|\Delta E| \approx 12.3kT$, *i.e.* considerably higher of the particles thermal energy at $T \sim 300$ K [47]. In other words, the separation of particles from the surface is hindered.

The initial layer of adsorbed particles grows due to Oswald effect and finally forms a layered shell [48, 49]. Its growth rate depends on particles diffusion rate in liquid. SDS presence in the solution will increase its viscosity, retard particle diffusion and, therefore, prevent the growth of shell sizes. Shell formation does not occur only because of small nanoparticles of zirconia. In the presence of SDS we can observe separate attached SDS crystallites and, possibly, crystallites of Zr–SDS composite (Fig. 5b). When drifting in the colloid nanostructures get to the area of laser beam it leads to fusion of their surface layer (Fig. 5c) [39, 50, 51]. It is noteworthy that high pulses repetition rate makes the generation of vapor-gas bubbles go very intensively, thus, the possibility of hollow nano and microstructure formation is increased. Kirkendall effect might be observed for particles with "nucleus-shell" structure, where the nucleus may be metal and the shell made of another material (metal oxide, *etc*.) [52-55], that leads to cavities formation inside particles due to differences of component diffusion rate. The formation time may make up to several minutes [52] and it goes down noticeably when particles are heated. In this regard, the appearance of such particles in the experiments is highly probable. Both effects can be a cause for appearing "rattle" structures (Fig. 5d) (smaller spheres are inside a lager one) [38]. It should be noted that the indicated hollow nano and micro-spheres at laser ablation of zirconium in water and aqueous solutions of SDS seem to be obtained for the first time.

3.4. Optical Characteristics. Absorption Spectra

Zirconia is a wide band gap insulator with two direct transmissions between zones of valence and conductivity of 5.2 and 5.79 eV [56]. Upper levels of the valence zone are mainly of O(2p) type and lower levels of the conductivity zone are determined by 4d orbitals zirconium ion Zr^{4+} [57, 58]. Changes of phase composition of ZrO_2 and the synthesis conditions, presence of surfactant, in particular, influence the absorption spectra that carry information about the structure of the formed crystalline lattice and its intrinsic and surface defects, vacancies, other inclusions [59, 60]. The investigation of absorption curves (Figs. 6 and 7) of the colloid solution obtained at 5 and 20 min target ablation in deionized water and aqueous SDS solution reveals some peculiar features of the spectrum:

- steep rise of absorption in UV range ~ 200–240 nm. The rise is observed both at M = 0 and M ≠ 0. When M = 0 the above mentioned zone of absorption can be

divided to two. The 200–220 spectrum region has a higher average absorption level and typical peaks at 200, 205, 210–212 nm, that are most dramatic at 5 min exposition (Fig. 6, *curve* 1), and the 220–240 nm region with the absorption level 20–25 % lower;

- zone of absorption rise (5–7 %) within the region of 240–350 nm with peaks at 270, 300, 325, and 350 nm (Fig. 6, *curves* 1, 3, 5; Fig. 7, *curves* 1, 3, 5, 6);
- absorption dips ("bleaching") in narrow spectrum interval at the beginning (245–255 nm) and at the end (~ 355 nm) of the mentioned region (Fig. 6, *curve* 1, 4, 5; Fig. 7, *curves* 3, 5, 6);
- increase (3–4 %) of absorption within the interval of 440–480 nm with maxima at 445, 460–470 nm (Fig. 6, *curves* 1, 4, 5).

The increase of ablation time and SDS concentration in solution gives a considerable rise of absorption level, especially in the long wave spectrum range, due to particle concentration growth. At that it does not change much within the wave range of 350–600 nm, which is typical of colloids with formed fractal structures of the solid phase [25, 61]. Colloid aging for 24 h and more does not practically change spectrum shape in the initial region of 200–260 nm (Fig. 6, Fig. 7 *curve* 3, 5). However, beyond this boundary the absorption decrease towards longer wave lengths is more dramatic, and the final level is considerably lower. That speaks to sedimentation of large units of the colloid solid phase.

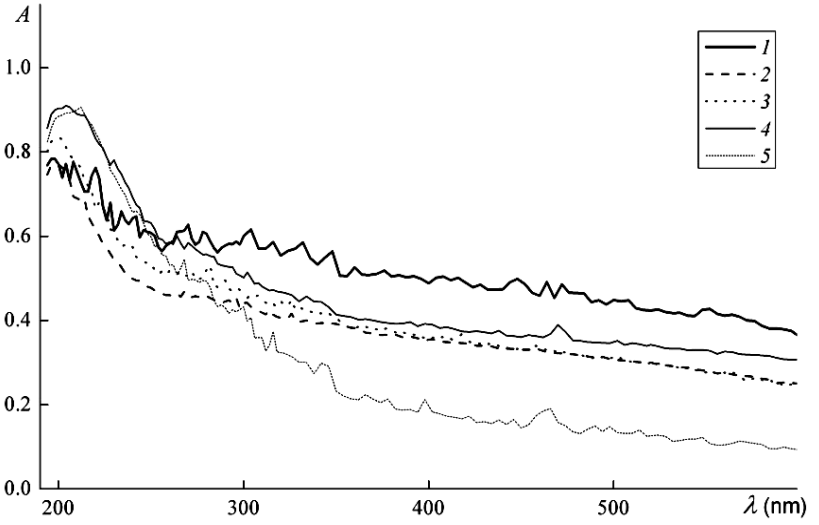

Fig. 6. Absorption spectra of $A(\lambda)t_{exp}$ = 5 min depending on the concentration (M) SDS: 0 (1); 0.01 (2); 0.01 (20 h aging) (3); 0.1 (4) and 0.1 (48 h aging) (5)

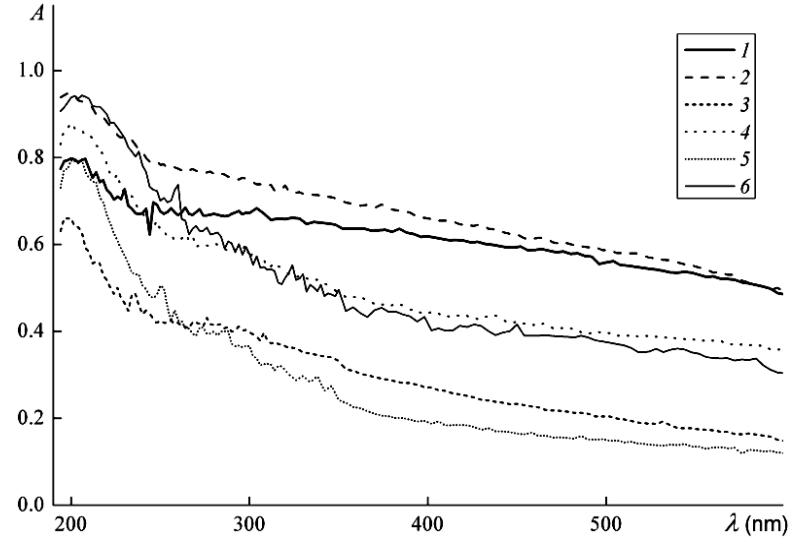

Fig. 7. Absorption spectra of $A(\lambda)t_{exp}$ = 20 min depending on the concentration (M) SDS: 0 (1); 0.01 (2); 0.01 (48 h aging) (3); 0.05 (4); 0.05 (48 h aging) (5) and 0.1 M (6)

The analysis of the mentioned features of the absorption spectrum with consideration of the phase mixture (cubic, monoclinic and tetragonal phases) and dimensional composition of ZrO_2 nanoparticles (40–100 nm) leads to the following conclusions. The steep rise of absorption in UV range from 200 to 240 nm seems to be associated to $O^{2-}(2p) \rightarrow Zr^{4+}(4d)$ transitions. Similar phenomenon was observed in a number of other researches [56, 57]. The spectrum region at 200–220 nm is determined by the presence of cubic and tetragonal phases, and of metal zirconium, as well. It is shown by typical absorption peaks at 200, 205, 210–212 nm [62, 63]. The appearance of monoclinic phase means the transformation of crystalline lattice structure, its symmetry. Coordination number of zirconium ions at transition from tetragonal to monoclinic phase changes from 8 to 7. This change leads to a split of 4d levels of Zr^{4+} ion and the appearance of long wave branch in $O^{2-}(2p) \rightarrow Zr^{4+}(4d)$ transition spectrum, *i.e.* the boundary of absorption band shifts to the red region up to 240–250 nm [56].

The band gap of zirconia E_g is calculated from the dependence of the absorption coefficient (α) on the photon energy (hv) in the band-edge spectral region for a direct transition by a known formula:

$$ahn = const\left(hn - E_g^{bulk}\right)^{1/2} \quad (1)$$

where h is Plank constant, E_g^{bulk} is the band gap of the solid [64].

It gives values for samples obtained at ablation on deionized water ~ 5.27 and 5.76 eV that is close to the mentioned above. The increase of SDS concentration in solution up to M = 0.1 reduces E_g to the level of ~ 4.54 and 4.78 eV. This fact is determined by growth of lattice defects at $M \neq 0$.

Zirconia, representing photoresistant metal oxides, possesses a typical property to capture charge carriers (electrons and holes) by crystalline lattice defects [65] with the formation of centers of absorption (F, V colour centers) or luminescence [65, 66]. Under the influence of radiation of a certain wavelength range the captured electrons or holes get free and recombine, in particular, by radiative emission, *i.e.* color (absorption) centers disappear. In that case gaps ("bleaching" zones) appear in absorption spectrum within rather narrow wavelength range. We should note that the process of nanostructure synthesis at metal ablation in liquid by nanosecond pulses is far from equilibrium. The presence of SDS molecules and ions in the solution also increases potential generation of defects inside and on the surface of crystals. Taking this into account, gaps in spectra presented in *curves* 1, 4, 5 (Fig. 6) and 3, 5, 6 (Fig. 7) at wavelengths of 245–255 nm and ~ 355 nm, enhanced absorption in regions of 240–350 nm, 440–480 nm and 540–600 nm can be attributed to the discussed above character. Similar facts were observed and discussed in [59].

3.5. Photoluminescence

Figs. 8 and 9 give colloid spectra obtained at different excitation wavelengths and SDS molar fractions in the initial solution. The spectra (Fig. 7, *curves* 1, 3) excited by UV radiation (λ_{exc} = 271 nm) in colloids with M = 0.05 and 0.1 take up a rather continuous region in the wavelengths of 340–610 nm. In both cases two parts are obviously specific: 310–400 nm and 400–535 nm. Maximal level of the signal in the second region is about 1.5–2.0 times higher. Moreover, luminescence intensity for the spectrum in general at M = 0.1 is higher than at M = 0.05. In the absence of SDS, firstly, the general level of luminescence goes down by several times and secondly, the spectrum starts from 330 nm. In this case we can see several regions of enhanced luminescence: 360, 420–425, 435–450 nm. Spectra maxima at $M \neq 0$ are shifted into the red region by ~ 50–60 nm and have flatter wide top. In the spectrum (Fig. 8) the luminescence region lies at 530 up to 575–580 nm at M = 0.01, while at M = 0 there is no luminescence. When analyzing causes of luminescence in colloids, it seems appropriate to consider a chain of processes mentioned in [59]:

$$Z \div hv_{ex} \rightarrow Z^* \quad (2)$$

$$Z^* \rightarrow Z \div hv_{lum} \quad (3)$$

$$Z \div hv_{ex} \rightarrow Z^+ + e \text{ (photoionization of defects, } Z) \quad (4)$$

$$Z^* \rightarrow Z^+ + e \text{ (thermal ionization of defects, } Z^*) \quad (5)$$

$$Z^+ + e \rightarrow (Z^*) \rightarrow Z + hv_{lum} \quad (6)$$

where Z and Z^* are basic and excited states of luminescence centers, process (6) is recovery of Z state by means of electron capture.

With consideration of conditions of ZrO_2 nanostructure synthesis processes (2)–(6) seem very probable in the present experiment. Introduction of SDS into the initial solution may considerably increase the number of intrinsic and, especially, surface defects, different vacancies, precondition appearance of new centers of absorption and luminescence in nanocrystals obtained after ablation. The indicated circumstances at $M \neq 0$ seem to determine a considerable growth of luminescence, enlargement of its spectrum to UV and red regions at λ_{exc} = 271 nm, and appearance of luminescence at λ_{exc} = 510 nm. It should be noted that the obtained data both in the wavelength range and in luminescence intensity coincide with the results of a number of researches, where synthesis of zirconia was performed by different chemical methods [60, 67-69].

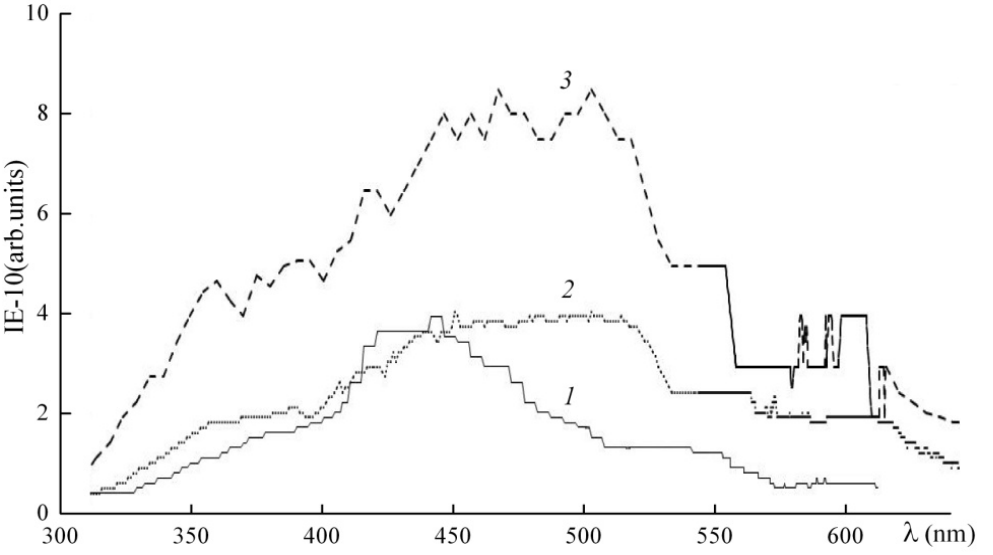

Fig. 8. Photoluminescence spectra of colloid depending on the concentration (M) SDS λ_{exc} = 271 nm: 0 (1); 0.05 (2) and 0.1 (3)

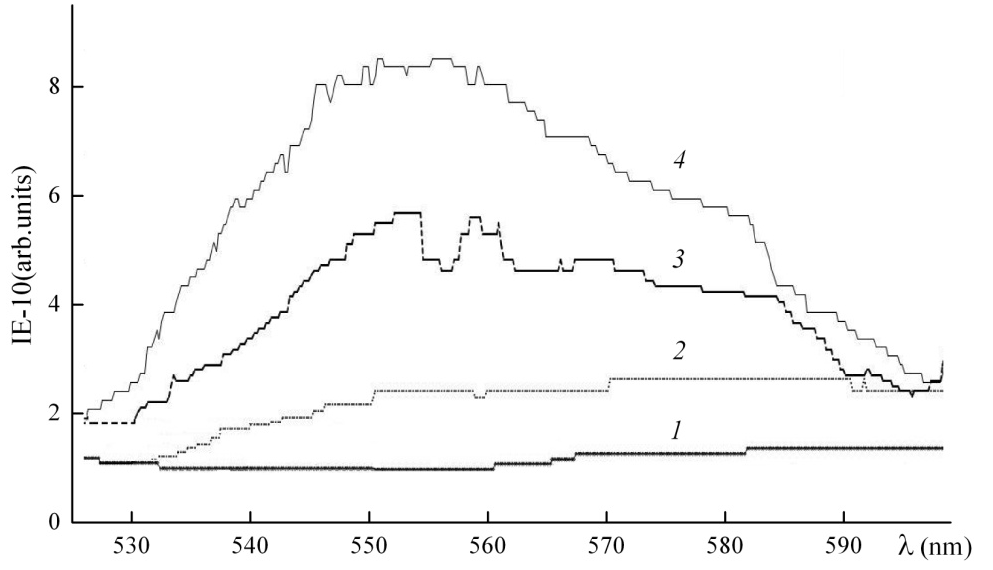

Fig. 9. Photoluminescence spectra of colloid depending on the concentration (M) SDS λ_{exc} = 510 nm: 0 (1); 0.01 (2); 0.05 (3) and 0.1 (4)

4. Conclusions

In the present research ZrO_2 nanostructure synthesis was performed by laser ablation under conditions of increased pulse repetition rate onto zirconium target both in deionized water and aqueous solutions of SDS. That mode provides optimal conditions for productive generation of zirconia and permits a relatively flexible transformation of properties in the obtained product. XRD data and RAMAN spectra point out an interesting feature of the experiment, *i.e.* prevalence of dioxide amorphous phase in the product of synthesis and the presence of all three ZrO_2 phases: cubic, tetragonal and monoclinic in the crystallized part of colloid. Application of surfactant SDS in the process of zirconia producing can be treated as an additional factor of stabilization for high temperature cubic and tetragonal phases. Besides, it seems that the fact of synthesizing organic-inorganic nanocomposites based on zirconium oxides or hydroxides and SDS alkyl chains was fixed in the experiment for the first time. The metal zirconium ablation in deionized water for the first time produced

hollow nano and microspheres from zirconia. The authors assume that a basic mechanism for their formation is the adsorption of particles on the surface of vapor-gas bubbles and Kirkendal effect cannot be excluded, as well. There are certain references [70] that similar structures are rather promising for practical application in biomedicine, pharmacology, for developing new materials, etc.

References

[1] Shukla S., Seal S. and Vanfleet R.: J. Sol-Gel Sci. Technol., 2003, **27**, 119.
[2] Salavati-Niasarim M., Dadkhah M. and Davar F.: Inorg. Chem. Acta, 2009, **362**, 3969.
[3] Feng X., Bai Y., Lu B. *et al.*: J. Cryst. Growth, 2004, **262**, 420.
[4] Ray J., Pramanik P. and Ram S.: Mater. Lett., 2001, **48**, 281.
[5] Sliem M., Schmidt D., Betard A. *et al.*: Chem. Mater., 2012, **24**, 4274.
[6] Tok A., Boey F., Du S. and Wong B.: Mater. Sci. Eng. B., 2006, **130**, 114.
[7] Meskin P., Ivanov V., Barantchikov A. *et al.*: Ultrasonics Sonochem., 2006, **13**, 47.
[8] Chen L., Mashimo T., Omurzak E. *et al.*: J. Phys. Chem. C., 2011, **115**, 9370.
[9] Cao G.: Nanostructures and nanomaterials: Synthesis, Properties and Applications. Imperial College Press, London 2004.
[11] Botta S., Navio J., Hidalgo M. *et al.*: J. Photochem. Photobiol. A, 1999, **129**, 89.
[12] Subbarao E. and Maiti H.: Adv. Ceram., 1988, **24**, 731.
[13] Latha Kumari, Du G., Li W. *et al.*: Ceramics Int., 2009, **35**, 2401.
[14] Varaksin A. Protasov M. and Teplitsky Yu.: High Temperature, 2014, **52**, 581.
[15] Kumar B., Thareja R.K.: J. Appl. Phys., 2010, **108**, 064906.
[16] Stratakis E., Zorba V., Barberoglou M. *et al.*: Appl. Surf. Sci., 2009, **255**, 5346.
[17] Liu P., Cai W., Fang M. *et al.*: Nanotechnology, 2009, **20**, 285707.
[18] Dezhi Tan, Geng Lin, Yin Liu *et al.:* J. Nanopart. Res., 2011, **13**, 1183.
[19] Dezhi Tan, Yu Teng, Yin Liu *et al.*: Chem. Lett., 2009, **38**, 1102.
[20] Mahmoud A., Fadhill Z., Ibrahim Al-Nassar S. *et al.*: J. Mat. Sci. and Eng. B3, 2013, **6,** 364.
[21] Chao-Hsien Wu, Chang-Ning Huang, Pouyan Shen *et al.*: J. Nanopart. Res., 2011, **13**, 6633.
[22] Golightly J. and Castleman A.: Zeitschrift für Physikalische Chemie, 2010, **221**, 1455.
[23] Simakin A., Voronov V. and Shafeev G.: Phys. of Wave Phenomena, 2007, **15**. 218.
[24] Bozon-Verduraz F., Brayner R., Voronov V. *et al.*: Quantum Electron., 2003, **33**, 714.
[25] Yang G.: Progress in Mater. Sci., 2007, **52**, 648.
[26] Karpuhin V., Malikov M., Val'yano G. *et al.:* High Temperature, 2011, **49**, 681.
[27] Batenin V., Bokhan P., Buchanov V. *et al.*: Lazery na Samoogranichennykh Perekhodakh Atomov Metallov-2. Publ. House of Physics, Moskva 2011.
[28] Stefanic G. and Music S.: Croatica Chem. Acta, 2002, **75**, 727.
[29] Li C. and Li M.: J. Raman Spectrosc., 2002, **32**, 301.
[30] Pesika N., Hu Z., Stebe K. and Searson P.: J. Phys. Chem, B, 2002, **106**, 6985.
[31] Kandare E., Chigwada G., Wang D. *et al.*: Polymer Degradation and Stability, 2006, **91**, 1781.
[32] Huo Q., Margolese D., Ciesla U. *et al.*: Chem. of Mater, 1994, **6**, 1176.
[33] Karpukhin V., Malikov M., Val'yano G. *et al.*: J. Nanotechnol., 2012**,** Article ID 910761 (2012); doi: 10.1155/2012/910761.
[34] Borodina T., Val'yano G., Gololobova O. *et al.*: Quantum Electron., 2013, **43**, 563.
[35] Smith L., Duncan A., Thomson G. *et al.*: J. Crystal Growth, 2004, **263**, 480.
[36] Yan Z., Bao R., Wright R. and Chrisey D.: Appl. Phys. Lett., 2010, **97**, 124106.
[37] Yan Z., Bao R., Huang Y. *et al.*: J. Phys. Chem. C, 2010, **114**, 3869.
[38] Yan Z., Bao R., Huang Y. and Chrisey D.: J. Phys. Chem. C, 2010, **114,** 11370.
[39] Yan Z., Bao R. and Chrisey D.: Nanotechnology, 2010, **21**, 145609.
[40] Lim K., Quinto-Su P., Klaseboer E. *et al.*: Phys. Rev. E, 2010, **81**, 016308.
[41] Yavas O., Leiderer P., Park H. *et al.*: Phys. Rev. Lett., 1993, **70**, 1830.
[42] Ohl C., Lindau O. and Lauterborn W.: Phys. Rev. Lett., 1998, **80**, 393.
[43] Brenner M.: Rev. of Modern Phys, 2002, **74**, 425.
[44] Li X., Shimizu Y., Pyatenko A. *et al.*: Nanotechnology, 2012, **23**, 115602.
[45] Takeda S., Ikuta Y., Hirano M. and Hosono H.: J. Mater. Res., 2001, **16**, 1003.
[46] Pyatenko A., Yamaguchi M. and Suzuki M.: J. Phys. Chem. C, 2007, **111**, 7910.
[47] Binks B.: Current Opinion in Colloids and Interface Sci., 2002, **7**, 21.
[48] Ostwald W.: Lehrbuch der Allgemeinen Chemie, v.2, Leipzig 1896.
[49] Ratke L. and Voorhees P.: Growth and Coarsening: Ostwald Ripening in Material Processing. Springer 2002.
[50] Orru R., Licheri R., Locci A. *et al.*: Mater. Sci. .Eng. R., 2009, **63**, 127.
[51] Kang Suk-Joong L.: Sintering: Densification, Grain Growth, and Microstructure. Elsevier Ltd. 2005.
[52] Smigelskas A. and Kirkendall E.: Trans. AIME, 1947, **171**, 130.
[53] Niu K., Park J., Zheng H. and Alivisatos A.: Nano Lett., 2013, **13**, 5715.
[54] Niu K., Yang J., Kulinich S. *et al.*: Langmuir, 2010, **26**, 16652.
[55] Yang J., Hou J. and Du X. School of Materials Science and Engineering. Tianjin: Tianjin University, 2013, 300072.
[56] Bluvshtein Z., Nizhnikova G. and Farberovich U.: Sov. Phys. Solid State, 1990, **32**, 548.
[57] Lopez E., Escribano V., Panizza M. *et al.*: J. Mater. Chem., 2001, **11**, 1891.
[58] Sutton D.: Electronic Spectra of Transition Metal Complexes. McGraw-Hill, New York 1968.
[59] Emeline A., Kataeva G., Litke A. *et al.*: Langmuir, 1998, **14**, 5011.
[60] Cong Y., Li B., Yue S. *et al.*: J. Phys. Chem. C., 2009, **113**, 13974.

[61] Karpov S. and Slabko V.: Opticheskie i Fotofizicheskie Svoistva Fractalno-Structuririvannykh Zolei Metallov. Ros. Acad. Nauk, Novosibirsk 2003.
[62] Sahu H. and Rao G.: Bull. Mater. Sci., 2000, **23**, 349.
[63] Geethalakshmi K., Prabhakaran T. and Hema: J. World Academy of Sci. Eng.Tech., 2012, **64,** 150.
[64] Pankove J.: Optical Properties in Semiconductors. Prentice Hall, Englewood Cliffs, NJ 1971.
[65] Lushchik Ch. and Lushchik A.: Elektronnye Vozbuzhdeniya s Obrazovaniem Defectov v Tverdykh Telakh. Nauka, Moskva 1989.
[66] Strekalovsky V., Polezhaev Yu. and Palguev S.: Oksidy s Primesnoi Razuporyadochennostiu: Sostav, Structura, Fazovye Prevrashcheniya. Nauka, Moskva 1987.
[67] Sliem M., Schmidt D., Betard A. *et al.*: Chem. Mater., 2012, **24**, 4274.
[68] Reddy Channu V., Kalluru R., Schlesinger M. *et al.*: Coll. Surf. A: Physicochem. Eng. Aspects, 2011, **386**, 151.
[69] Neppolian B., Wang Q., Yamashita H. and Choi H.: Appl. Catal. A, 2007, **333**, 264.
[70] Zhou J., Wu W., Caruntu D. *et al.*: J. Phys. Chem. C., 2007, **111**, 17473.

Received: September 16, 2014 / Revised: October 18, 2014 / Accepted: May 21, 2015

СТРУКТУРНІ, МОРФОЛОГІЧНІ ТА ОПТИЧНІ ВЛАСТИВОСТІ НАНОПРОДУКТІВ ЛАЗЕРНОЇ АБЛЯЦІЇ ЦИРКОНІЄВОЇ МІШЕНІ У ВОДІ ТА ВОДНИХ РОЗЧИНАХ SDS

Анотація. *Досліджено структурні, морфологічні та оптичні властивості нанопродуктів лазерної абляції цирконієвої мішені у воді та водних розчинах SDS. Залежно від експериментальних умов зазначені продукти отримані у вигляді оксидів у різноманітних фазових станах і органо-неорганічних композитів, які являють собою структури з алкільними ланцюгами SDS та знаходяться між шарами оксидів або гідроксидів. Показано утворення близьких до сферичних, порожнистих нано- і мікроструктур з діоксиду цирконію. Висунуте припущення, що газа-парові пузирі, які утворюються в процесі абляції, є темплетами для генерації порожнистих структур.*

Ключові слова: *лазерна абляція, нанокомпозит, ZrO_2, рамановські спектри.*